# Chapter 2 Waveguide laser theory

## 2.1 Introduction

This chapter introduces the theoretical concepts underpinning the work described in this thesis. The chapter is subdivided into three sections. The first section describes the propagation of light in a planar waveguide using the simple model of a slab waveguide. The model deals with a general five-layer asymmetric slab structure and is then applied to the simpler cases of a three-layer asymmetric slab structure and a symmetric five-layer structure. Both types of planar waveguide have been used experimentally in the work discussed in this thesis. The second section contains details of bulk laser theory and the modelling of threshold and slope efficiency for three- and four-level laser systems. This is then modified to account for a waveguide geometry, and the theoretical performance of bulk and waveguide lasers are compared. The final section discusses how to define waveguide laser beam quality.

## 2.2 Optical waveguide theory

The propagation modes of a waveguide structure are very important in determining the properties of a waveguide laser. For example the lasing modes propagating in the waveguide define the output beam quality, and the laser threshold and efficiency characteristics are dependant on both the pump and signal mode sizes and overlap.

There are many ways in which to describe the propagation of light in a waveguide. Numerous textbooks [1,2,3,4,5] deal with the task and merely an introduction to the subject will be given here. The analysis used in this chapter is similar to that described by Yariv [1] and Lee [2]. It is restricted here to finding the propagation modes of structures with one dimensional guidance. Details of other approaches are given in the references and include; classical propagating ray analysis based on geometrical optics [3], the WKB method [4] for graded refractive index waveguides, and other numerical beam propagation methods [5].

### 2.2.1 Five-layer asymmetric slab waveguide

The three-layer asymmetric slab waveguide considered in many textbooks is one of the most straightforward geometries to examine. However some of the waveguides examined during the course of this thesis consisted of five layers. In order to investigate these structures a general five-layer asymmetric slab (planar) model has been developed and then generalised to a five-layer symmetric, and a three-layer asymmetric case.

A schematic diagram of the asymmetric structure is shown in figure 2.1. The elements of the waveguide are; a substrate (region 5), considered infinitely thick in this analysis, a thin inner cladding layer of a higher refractive index than the substrate (region 4), a thin, high-index core layer (region 3), an outer cladding layer (region 2) and a superstrate (region 1), which is also considered to be infinitely thick.

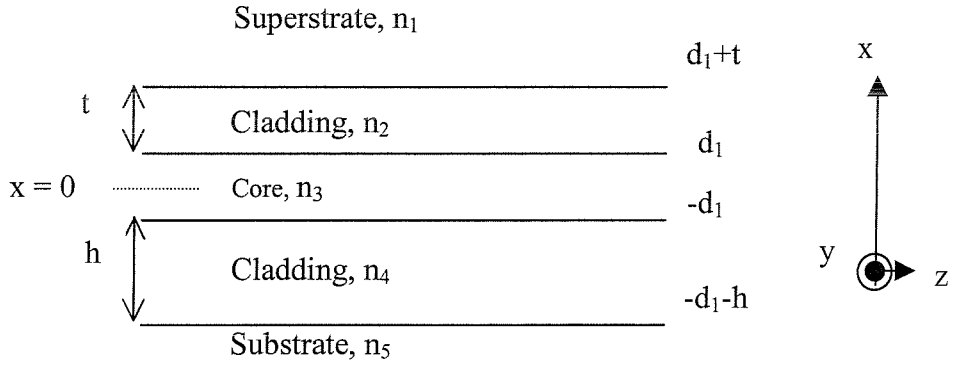


*Figure 2.1* Schematic diagram of an asymmetric slab waveguide

The light propagates in the z-direction and is confined in the waveguide by total internal reflection (TIR) at the core-cladding interface or at the cladding-superstrate and cladding-substrate interfaces. TIR at an interface between two media means that the angle of propagation, $\theta_p$, in the bouncing-beam model (as shown in figure 2.2) must be greater than the critical angle, $\theta_c$, for the interface. If this is true then the light is described as travelling in a guided mode, where p is the mode number.

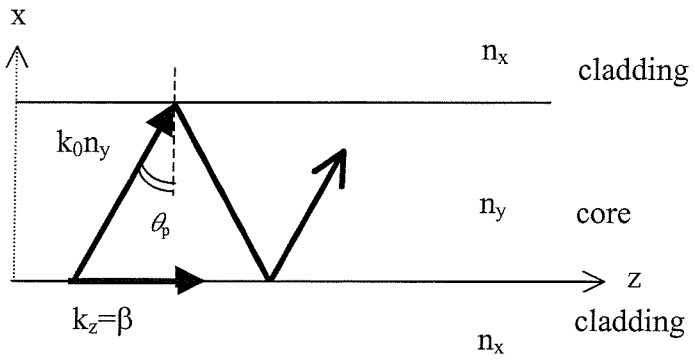


*Figure 2.2* Diagram illustrating TIR and the propagation constant β

The overall condition for guidance in the structure shown in figure 2.1 is, $n_3>n_2,n_4>n_1,n_5$, where the refractive index of a region m is given by $n_m$, i.e. the refractive index of a region must be greater than the refractive indices of the cladding layers, which are in turn greater than those of the superstrate and substrate layers. For instance TIR would occur at the core-cladding boundary of figure 2.2 when $\theta_p$ was greater than $\theta_c$ given by equation 2.1 (from Snell's law).

$$\theta_c = \sin^{-1}\left(\frac{n_x}{n_y}\right) \qquad 2.1$$

Waveguide theory is often not formulated in terms of the propagation angle $\theta_p$, but in terms of β, the propagation constant. Figure 2.2 illustrates β, which is related to the optical path length seen by the guided mode. The propagation constant in the direction in which the wavefront moves is given by $k_0n_y$, where the wavenumber, $k_0 = 2\pi/\lambda$ and $\lambda$ is the wavelength of the light in free space. The propagation constant along the guided (z) direction is therefore:

$$k_z = k_0 n_y \sin\theta_p = \beta \qquad 2.2$$

The quantity $n_y\sin\theta_p$ in equation 2.2 is often labelled $n_{eff}$ and is known as the effective index of a mode. Thus the propagation constant can be rewritten as:

$$\beta = k_0 n_{eff} \qquad 2.3$$

For the guidance condition to be satisfied $\theta_p$ must be greater than $\theta_c$ and so $n_{eff}$ must satisfy the condition $n_3 > n_{eff} > n_1, n_5$.

In order for the mode to maintain its shape as it propagates along z, β must be the same in all five layers. Propagation constants can be defined for the +x and –x directions in the core, cladding, superstrate and substrate regions. The propagation constants in the ±x direction in the core describe an oscillatory TIR wave. The propagation constants in the ±x direction in the cladding describe, both the oscillatory nature of the guided wave when $n_2, n_4 > n_{eff} > n_1, n_5$ and the rate of decay of the evanescent field with distance from the core boundary when $n_{eff} > n_2, n_4$. While in the substrate and superstrate the ±x direction propagation constants represent only the rate of decay of the evanescent field, as $n_{eff}$ is always greater than $n_1, n_5$.

Electromagnetic waves propagating in the five-layer structure obey Maxwell's equations and these equations form the basis of the following analysis. Equations 2.4 – 2.7 show Maxwell's equations in their general form:

$$\underline{\nabla} \times \underline{E}(\underline{r}, t) = -\frac{\partial \underline{B}(\underline{r}, t)}{\partial t} \qquad 2.4$$

$$\underline{\nabla} \times \underline{H}(\underline{r}, t) = \frac{\partial \underline{D}(\underline{r}, t)}{\partial t} + \underline{J}(\underline{r}, t) \qquad 2.5$$

$$\underline{\nabla} \bullet \underline{D}(\underline{r}, t) = \rho(\underline{r}, t) \qquad 2.6$$

$$\underline{\nabla} \bullet \underline{B}(\underline{r}, t) = 0 \qquad 2.7$$

where, $\underline{E}$, $\underline{H}$ are electric and magnetic fields respectively.

$\underline{D}$ is the electric displacement vector.

$\underline{B}$ is the magnetic flux density.

$\rho$, $\underline{J}$ are the charge and current densities respectively.

t is time, $\underline{r}$ is a position vector in space.

$\underline{D}$ and $\underline{E}$ are related by $\underline{D} = \varepsilon_0\varepsilon_r\underline{E} = \varepsilon\underline{E}$, and $\varepsilon_0$, $\varepsilon_r$ are respectively the permittivity of free space and the relative permittivity of the material. Also, $\underline{B} = \mu_0\mu_r\underline{H} = \mu\underline{H}$, where $\mu_0, \mu_r$ are the permeability of free space and the relative permeability of the medium respectively.

Assuming there is no current flow (no current sources present) in the material, $\underline{J}=0$, equations 2.4 and 2.5 can be rewritten in terms of $\underline{E}$ and $\underline{H}$ only:

$$\underline{\nabla} \times \underline{E}(\underline{r},t) = -\frac{\partial}{\partial t}\mu\underline{H}(\underline{r},t) \qquad 2.8$$

$$\underline{\nabla} \times \underline{H}(\underline{r},t) = \frac{\partial}{\partial t}\varepsilon\underline{E}(\underline{r},t) \qquad 2.9$$

For a transverse electric (TE) polarised wave (with $\underline{E}$ orientated along the $\underline{y}$ direction) the $\underline{E}$-field can be separated into its spatial and temporal components:

$$\underline{E}(\underline{r},t) = E_y(x,z)e^{i\omega t} \qquad 2.10$$

where $\omega$ is angular frequency, and the field variations are independant of y.

The TE modes only are considered for analysis here. These show the general behaviour of modes in the waveguide and in practice, the polarised laser outputs obtained during the course of this work were found to be TE polarised (see results in chapter 7). The solution to Maxwell's equations in each of the five layers, should lead to oscillatory solutions only in region 3, evanescent solutions only in regions 1 and 5, and both types of solution in regions 2 and 4.

The spatial component of the $\underline{E}$-field can therefore be characterised in the five regions as follows:

$$E_y(x,z) = \begin{Bmatrix} E_1 e^{-\alpha_1 x} \\ E_2 e^{-\alpha_2 x} + E_2' e^{\alpha_2 x} \\ \cos(kx + \Psi) \\ E_4 e^{\alpha_4 x} + E_4' e^{-\alpha_4 x} \\ E_5 e^{\alpha_5 x} \end{Bmatrix} e^{-ik_z x} \quad \text{in the regions} \quad \begin{cases} x \geq d_1 + t \\ d_1 \leq x < d_1 + t \\ -d_1 \leq x < d_1 \\ -(d_1 + h) \leq x < -d_1 \\ x < -(d_1 + h) \end{cases}$$

2.11

where $E_1$, $E_2$, $E_2$', $E_4$, $E_4$' $E_5$, are electric field amplitude coefficients

$\Psi$ is a phase offset

$k_z$ is the wave number in the z direction

$\alpha_1$, $\alpha_2$, k, $\alpha_4$, $\alpha_5$ are transverse wave numbers obtained from the solution of the wave equation, derived from Maxwell's equations in each region.

$$\nabla^2 \underline{E}(\underline{r},t) = -\mu\varepsilon \frac{\partial^2}{\partial t^2} \underline{E}(\underline{r},t) \qquad 2.12$$

with: $\alpha_1 = \sqrt{k_z^2 - \omega^2 \mu_1 \varepsilon_1}$ 2.13

$\alpha_2 = \sqrt{k_z^2 - \omega^2 \mu_2 \varepsilon_2}$ 2.14

$k = \sqrt{\omega^2 \mu_3 \varepsilon_3 - k_z^2}$ 2.15

$\alpha_4 = \sqrt{k_z^2 - \omega^2 \mu_4 \varepsilon_4}$ 2.16

$\alpha_5 = \sqrt{k_z^2 - \omega^2 \mu_5 \varepsilon_5}$ 2.17

where $\varepsilon_m$, $\mu_m$, are, respectively, the permittivity and permeability of region m.

Equations 2.13 –2.17 can also be expressed as

$$\alpha_m = k_0 \sqrt{n_{eff}^2 - n_m^2} \qquad 2.18$$

and

$$k = k_0 \sqrt{n_3^2 - n_{eff}^2} \qquad 2.19$$

where $k_0 = \omega\sqrt{\mu_0 \varepsilon_0}$ and $n_m = \sqrt{\frac{\varepsilon_m}{\varepsilon_0}}$

In order to find the relative field amplitude coefficients the boundary conditions that $E_y$ and $H_z$ are continuous across the layer interfaces must be used [1], i.e $E_y$ and $H_z$ are continuous across the planes $-d_1$, $-(d_1+h)$, $d_1$ and $d_1+t$. $H_z$ is found from equation 2.8:

$$H_z(x,z) = \frac{i}{\omega\mu}\frac{\partial}{\partial x}E_y(x,z) \qquad 2.20$$

Application of the boundary conditions produces a set of simultaneous equations which can then be solved to obtain solutions 2.21-2.26

$$E_1 = \frac{\left[1+\left(\frac{\alpha_2-\alpha_1}{\alpha_2+\alpha_1}\right)\right]\cos(kd_1+\Psi)e^{-\alpha_2 t}}{\left[1+\left(\frac{\alpha_2-\alpha_1}{\alpha_2+\alpha_1}\right)e^{-2\alpha_2 t}\right]e^{-\alpha_1(d_1+t)}} \qquad 2.21$$

$$E_2 = \frac{\cos(kd_1+\Psi)e^{\alpha_2 d_1}}{\left[1+\left(\frac{\alpha_2-\alpha_1}{\alpha_2+\alpha_1}\right)e^{-2\alpha_2 t}\right]} \qquad 2.22$$

$$E_2' = \frac{\left(\frac{\alpha_2-\alpha_1}{\alpha_2+\alpha_1}\right)\cos(kd_1+\Psi)e^{-\alpha_2(d_1+2t)}}{\left[1+\left(\frac{\alpha_2-\alpha_1}{\alpha_2+\alpha_1}\right)e^{-2\alpha_2 t}\right]} \qquad 2.23$$

$$E_4 = \frac{\cos(-kd_1+\Psi)e^{\alpha_4 d_1}}{\left[1+\left(\frac{\alpha_4-\alpha_5}{\alpha_4+\alpha_5}\right)e^{-2\alpha_4 h}\right]} \qquad 2.24$$

$$E_4' = \frac{\left(\frac{\alpha_4 - \alpha_5}{\alpha_4 + \alpha_5}\right)\cos(-kd_1 + \Psi)e^{-\alpha_4(d_1+2h)}}{\left[1+\left(\frac{\alpha_4 - \alpha_5}{\alpha_4 + \alpha_5}\right)e^{-2\alpha_4 h}\right]} \qquad 2.25$$

$$E_5 = \frac{\left[1+\left(\frac{\alpha_4 - \alpha_5}{\alpha_4 + \alpha_5}\right)\right]\cos(-kd_1 + \Psi)e^{-\alpha_4 h}}{\left[1+\left(\frac{\alpha_4 - \alpha_5}{\alpha_4 + \alpha_5}\right)e^{-2\alpha_4 h}\right]e^{-\alpha_5(d_1+h)}} \qquad 2.26$$

Evaluating boundary conditions at $x=d_1$ and using $\tanh x = \frac{e^x - e^{-x}}{e^x + e^{-x}}$ gives:

$$\tan(kd_1 + \Psi) = \left(\frac{\alpha_1\alpha_2 + \alpha_2^2 \tanh\alpha_2 t}{k\alpha_2 + k\alpha_1 \tanh\alpha_2 t}\right) \qquad 2.27$$

and similarly evaluating boundary conditions at $x=-d_1$ gives:

$$\tan(kd_1 - \Psi) = \left(\frac{\alpha_4\alpha_5 + \alpha_4^2 \tanh\alpha_4 h}{\alpha_4 k + \alpha_5 k \tanh\alpha_4 h}\right) \qquad 2.28$$

Using the relationship $\tan(x)=\tan(x \pm p\pi)$ where p is any integer, equations 2.27 and 2.28 can be combined to eliminate $\Psi$:

$$2kd_1 - \tan^{-1}\left(\frac{\alpha_4\alpha_5 + \alpha_4^2 \tanh\alpha_4 h}{\alpha_4 k + \alpha_5 k \tanh\alpha_4 h}\right) - \tan^{-1}\left(\frac{\alpha_1\alpha_2 + \alpha_2^2 \tanh\alpha_2 t}{\alpha_2 k + \alpha_1 k \tanh\alpha_2 t}\right) = p\pi \qquad 2.29$$

Equation 2.29 can be numerically solved in order to find a value for k, equations 2.13-2.17 can then be used to find the values of $k_z$, $\alpha_1$, $\alpha_2$, $\alpha_4$, $\alpha_5$ and $\psi$ is given by equations 2.27 and 2.28. Equation 2.29 is known as the mode guidance condition equation [1] for a mode number p.

This analysis has only considered the TE modes of the waveguide. Transverse magnetic (TM) solutions (where H is polarised along the y direction) can be found from the duality in Maxwell's equations [2].

### 2.2.2 Five-layer symmetric slab waveguide

In practice an asymmetric five-layer planar waveguide has not been fabricated or used during the course of the work described here, however the model developed in section 2.2.1 can now be generalised to describe a symmetric five-layer structure that was used in experiments described in chapter 7. A schematic diagram of the general symmetric five-layer waveguide structure is shown in figure 2.3.

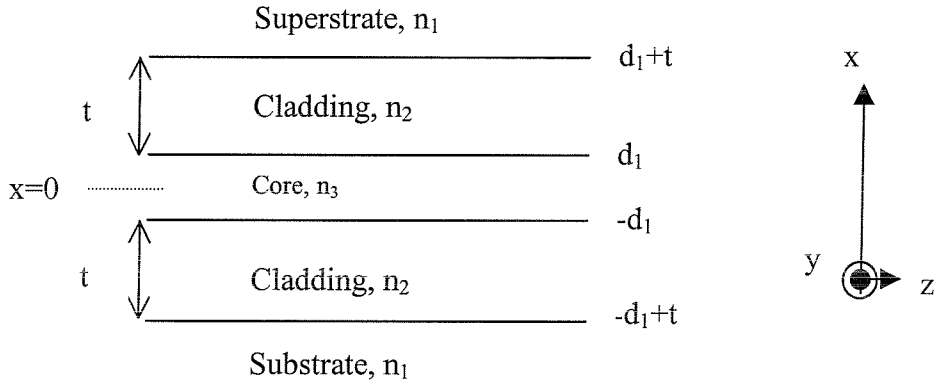


*Figure 2.3* Diagram of a five-layer symmetric waveguide

The five-layer, or double-clad, structure investigated in chapter 7 was composed of a thin (~10μm), high index core of rare-earth-doped YAG, a thin inner cladding (~10μm) of undoped YAG, and a thick (~500μm) outer cladding of Sapphire.

A symmetric structure is expected to have even ($\psi=0$) and odd ($\psi=\pi$) modes within its core. The mode guidance conditions for this geometry are as follows [6].
For the even modes:

$$\tan(kd_1) = \left( \frac{\alpha_1\alpha_2 + \alpha_2^2 \tanh\alpha_2 t}{k\alpha_2 + k\alpha_1 \tanh\alpha_2 t} \right) \qquad 2.30$$

and for the odd modes:

$$\cot(kd_1) = -\left(\frac{\alpha_1\alpha_2 + \alpha_2^2 \tanh\alpha_2 t}{k\alpha_2 + k\alpha_1 \tanh\alpha_2 t}\right) \qquad 2.31$$

These conditions can be seen as a special case of the mode guidance condition (2.29), where $\alpha_1=\alpha_5$, $\alpha_2=\alpha_4$, h=t and p=0,2,4.... for the even modes or p=1,3,5..... for the odd modes. Once again these conditions can be solved numerically.

### 2.2.3 **Three-layer asymmetric slab waveguide**

The most common type of waveguide structure examined in this thesis was the three-layer asymmetric planar waveguide. The light is confined to propagate within the core region by reflection at the boundaries with the substrate material and the cladding layer, which is often air. The condition for guidance is that the core index is greater than the cladding or substrate index.

Equation 2.29 can easily be generalised to a three-layer structure by setting h=0, t=0 and $\alpha_1=\alpha_2$, $\alpha_4=\alpha_5$ such that,

$$2kd_1 - \tan^{-1}\left(\frac{\alpha_1}{k}\right) - \tan^{-1}\left(\frac{\alpha_5}{k}\right) = p\pi \qquad 2.32$$

This is in agreement with other reported analysis [2].

## 2.3. Laser theory

### 2.3.1 Introduction

This section will discuss basic laser theory and apply the theory to a planar waveguide geometry. Comparisons between bulk lasers and waveguide lasers will be made. The laser system considered is shown in figure 2.4. This shows the energy level diagram for a typical four-level laser system, such as the $^4F_{3/2} \rightarrow {}^4I_{11/2}$ 1.1μm transition in

neodymium which has been extensively investigated in this thesis. In a four-level laser system an incoming pump photon excites an electron from its low energy ground state to some higher energy excited state. This higher energy electron loses energy via a non-radiative decay process. It then occupies a metastable upper laser level and can undergo stimulated emission from here to a lower laser level. Finally the electron decays back to the ground state, via a non-radiative transition, and the cycle can start again.

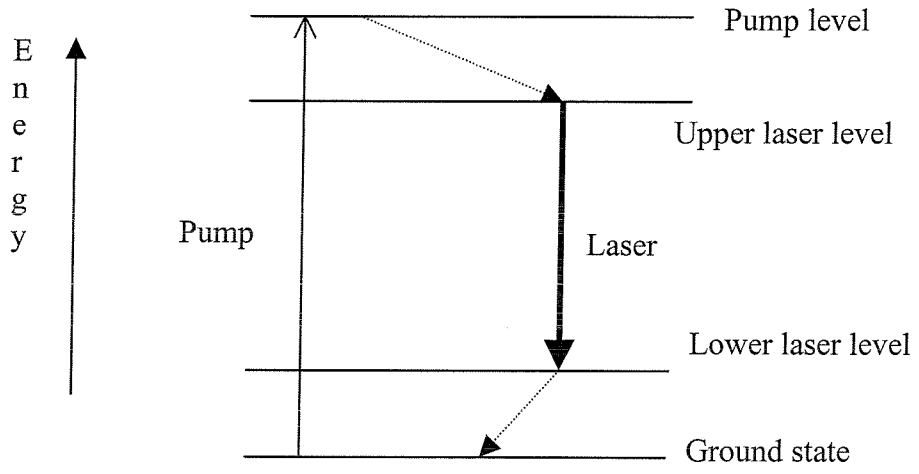


*Figure 2.4* Basic four-level laser system

Another type of laser system, known as quasi-three-level, operates when the lower laser level is part of the ground state manifold. Figure 2.5 shows the energy level diagram for this type of laser. Examples of quasi-three-level transitions include the $^4F_{3/2} \rightarrow {}^4I_{9/2}$ transition around 0.9μm in neodymium and the $^2F_{5/2} \rightarrow {}^2F_{7/2}$ transition around 1030nm in ytterbium, which have also been studied in this thesis. Three-level laser systems suffer from additional loss not present in four-level systems due to the thermally-populated lower laser level. Electrons in this level reabsorb laser photons that have undergone stimulated emission adding to the overall loss of the transition.

An analysis of a longitudinally-pumped quasi-three-level system will be used to derive expressions for the threshold and output power of a laser (following Risk [7] and Kubodera and Otuska [8]), allowing for the asymmetric mode-shape often found

in planar waveguides. This result will then be extended to apply to a four-level laser and to a side-pumped geometry.

### 2.3.2 Quasi-three-level lasers

The energy level diagram for a typical quasi-three-level laser is shown in figure 2.5.

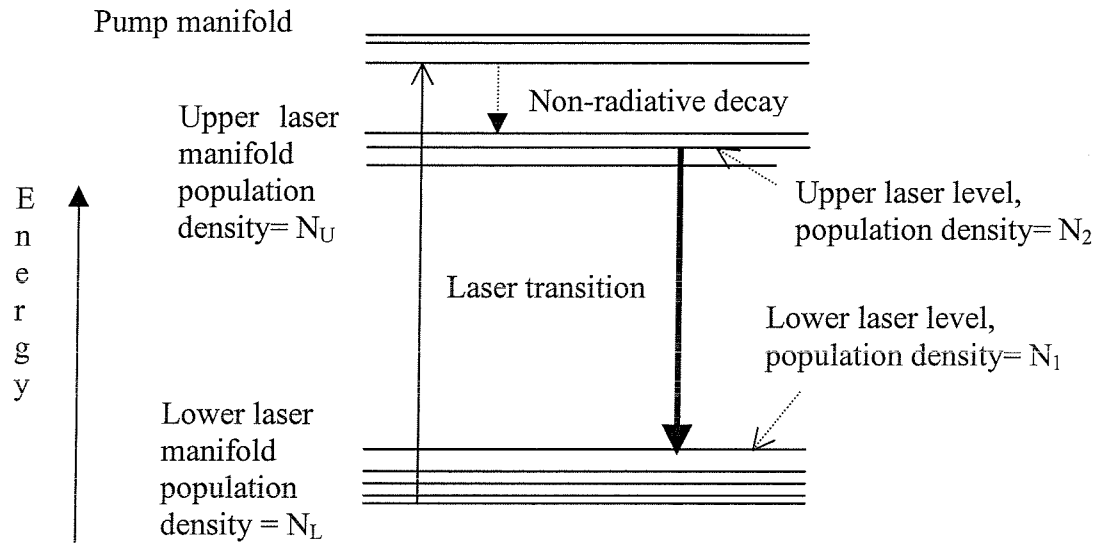


*Figure 2.5* Energy level diagram of a typical quasi-three-level transition

The lower laser level population density, $N_1$, can be expressed as $N_1 = f_1 N_L$, where $f_1$ is the fraction of the lower laser manifold population density residing in the appropriate Stark-level. Similarly $N_2$, the upper laser level population density, is given by $N_2 = f_2 N_U$, where $f_2$ is the fraction of $N_U$ in the Stark-level forming the upper laser level. The steady-state rate equations for $N_1$, $N_2$ and the population inversion density, $\Delta N = N_2 - N_1$, can now be written assuming negligible depletion of the ground state. In this analysis the effects of spatial hole burning are neglected [9] and the pump light is considered to make just one pass through the laser medium.

$$\frac{dN_1(x,y,z)}{dt} = -f_1 Rr(x,y,z) - \frac{N_1(x,y,z) - N_1^{\,0}}{\tau} + \frac{f_1 c \sigma_e [N_2(x,y,z) - N_1(x,y,z)]}{n} \Phi\phi(x,y,z) = 0 \qquad 2.33$$

$$\frac{dN_2(x,y,z)}{dt} = f_2 Rr(x,y,z) - \frac{N_2(x,y,z) - N_2{}^0}{\tau} - \frac{f_1 c\sigma_e[N_2(x,y,z) - N_1(x,y,z)]}{n}\Phi\phi(x,y,z) = 0 \qquad 2.34$$

By subtracting 2.33 from 2.34:

$$\frac{d\Delta N(x,y,z)}{dt} = (f_1 + f_2)Rr(x,y,z) - \frac{\Delta N(x,y,z) - \Delta N^{\,0}}{\tau} - \frac{(f_1 + f_2)c\sigma_e \Delta N(x,y,z)}{n}\Phi\phi(x,y,z) = 0 \qquad 2.35$$

where $\tau$ is the lifetime of the upper level, $\Delta N^0 = N_2{}^0 - N_1{}^0$ is the unpumped population inversion density, c is the speed of light in a vacuum, $\sigma_e$ is the laser emission cross section and n is the refractive index of the laser material.

R is the rate of pumping: $$R = \frac{P_p(1 - e^{-\alpha_p l})}{h\upsilon_p} \qquad 2.36$$

where it is assumed that the pump propagation losses in the waveguide are negligible compared to the absorption loss,

and $\Phi$ is the number of photons in the cavity: $$\Phi = \frac{2nlP_L}{ch\upsilon_L} \qquad 2.37$$

where $l$ is the length of the laser gain medium, $P_P$ is the incident pump power, $P_L$ is the intracavity laser power travelling in one direction, h is Planck's constant, $\upsilon_p$ and $\upsilon_L$ are the pump and laser frequencies respectively and $\alpha_p$ is the absorption coefficient of the pump in the gain medium.

r(x,y,z) and $\phi$(x,y,z) are respectively, the normalised pump and signal distributions such that:

$$\int_{\text{cavity}} r(x,y,z)dV = \int_{\text{cavity}} \phi(x,y,z)dV = 1 \qquad 2.38$$

writing $f=f_1+f_2$ and noting that $N_1^0>>N_2^0$ in thermal equilibrium, enables equation 2.35 to be rearranged to give [7]:

$$\Delta N(x,y,z) = \frac{f\tau R r(x,y,z) - N_1^0}{1 + \frac{c\sigma_e \tau}{n} f\Phi\phi(x,y,z)} \qquad 2.39$$

The growth in the propagating signal intensity, I(x,y,z), related to the gain, g(x,y,z) is given by [7]:

$$\frac{dI(x,y,z)}{dz} = g(x,y,z)I(x,y,z) \qquad 2.40$$

The laser condition stating that round-trip loss must equal round-trip gain in the cavity can be expressed as equation 2.41 for small values of loss.

$$\int_{\text{roundtrip}} dP_L(z) = 2\int_0^l \frac{dP_L(z)}{dz}dz = P_L(L+T) \qquad 2.41$$

where L is the round-trip cavity loss exponent excluding any mirror losses, and T is the natural logarithm of the output mirror reflectivity. T is approximately equal to the mirror transmission for high values of mirror reflectivity.

$P_L(z)$ is the single-pass intracavity power at a point z and is found by integration:

$$P_L(z) = \int_{-\infty}^{\infty}\int_{-\infty}^{\infty} I(x,y,z)\,dxdy \qquad 2.42$$

Differentiating 2.42 with respect to z gives:

$$\frac{dP_L(z)}{dz} = \int_{-\infty-\infty}^{\infty}\int^{\infty}\frac{dI(x,y,z)}{dz}dxdy \qquad 2.43$$

Using equations 2.40, 2.41 and 2.43:

$$2\int_0^l\int_{-\infty-\infty}^{\infty}\int^{\infty} g(x,y,z)\,I(x,y,z)\,dxdydz = P_L(L+T) \qquad 2.44$$

Equation 2.44 can then be rewritten using $\Delta N(x,y,z)$ from 2.39 and the expressions $g(x,y,z)=\sigma_e\Delta N(x,y,z)$ and $I(x,y,z)=\left(\frac{ch\upsilon_L}{2n}\right)\Phi\phi(x,y,z)$. Equation 2.45 then describes a bulk laser above threshold.

$$2\int_0^l\int_{-\infty-\infty}^{\infty}\int^{\infty}\frac{ch\upsilon_L}{2n}\left[\frac{f\sigma_e\tau Rr(x,y,z)-N_1{}^0\sigma_e}{1+\frac{c\sigma_e\tau}{n}f\Phi\phi(x,y,z)}\right]\Phi\phi(x,y,z)dxdydz = P_L(L+T) \qquad 2.45$$

### 2.3.3 Application to waveguide lasers

To apply equation 2.45 to a planar waveguide laser the values of $\phi(x,y,z)$ and $r(x,y,z)$, the normalised pump and signal distributions, must be evaluated. In a channel waveguide, or an optical fibre, it is assumed that the pump and signal spot size remain the same throughout the gain medium. However this is not the case for the non-guided plane of a thin-film waveguide. Instead the normalisation uses the approximation of an average spot size propagating in the non-guided plane of the gain medium. The normalised pump and signal distributions, calculated to satisfy the condition 2.38, are given in 2.46 and 2.47, where $w_{p(x,y)}$ are the pump beam spot sizes in the x (guided) and y (non-guided) directions respectively, and $w_{L(x,y)}$ are the corresponding signal beam spot sizes.

$$r(x,y,z) = \frac{2\alpha_p}{\pi w_{px} w_{py}(1-e^{-\alpha_p l})}\exp\left(\frac{-2x^2}{w^2{}_{px}}\right)\exp\left(\frac{-2y^2}{w^2{}_{py}}\right)\exp(-\alpha_p z) \qquad 2.46$$

$$\phi(x,y,z) = \frac{2}{\pi w_{Lx} w_{Ly} l} \exp\left(\frac{-2x^2}{w^2_{Lx}}\right) \exp\left(\frac{-2y^2}{w^2_{Ly}}\right) \qquad 2.47$$

These equations (2.46 and 2.47) are combined with 2.45, 2.36 and 2.37 to give:

$$2\int_0^l \int_{-\infty}^{\infty}\int_{-\infty}^{\infty} \frac{ch\upsilon_L \Phi}{2n} \frac{\left[\frac{2\sigma_e \tau f P_p \alpha_p}{h\upsilon_p \pi w_{px} w_{py}} \exp\left(\frac{-2x^2}{w^2_{px}}\right)\exp\left(\frac{-2y^2}{w^2_{py}}\right)\exp(-\alpha_p z) - N_1^0 \sigma_e\right]}{\left[1+\frac{2c\sigma_e \tau f \Phi}{n\pi w_{Lx} w_{Ly} l}\exp\left(\frac{-2x^2}{w^2_{Lx}}\right)\exp\left(\frac{-2y^2}{w^2_{Ly}}\right)\right]} \times$$

$$\frac{2}{\pi w_{Lx} w_{Ly} l} exp\left(\frac{-2x^2}{w^2_{Lx}}\right)\exp\left(\frac{-2y^2}{w^2_{Ly}}\right) dxdydz = \Phi \frac{ch\upsilon_L}{2nl}(L+T)$$

2.48

2.48 can be simplified with the substitutions 2.49 to the following (2.50):

$$a_{px} = \exp\left(\frac{-2x^2}{w^2_{px}}\right) \qquad a_{py} = \exp\left(\frac{-2y^2}{w^2_{py}}\right)$$

$$a_{Lx} = \exp\left(\frac{-2x^2}{w^2_{Lx}}\right) \qquad a_{Ly} = \exp\left(\frac{-2y^2}{w^2_{Ly}}\right) \qquad 2.49$$

$$\int_0^l \int_{-\infty}^{\infty}\int_{-\infty}^{\infty} \frac{\left[\frac{2\sigma_e \tau f P_p \alpha_p}{\pi h\upsilon_p w_{px} w_{py}}(a_{px})(a_{py})\exp(-\alpha_p z) - N_1^0 \sigma_e\right]\left[\frac{4}{\pi w_{Lx} w_{Ly}}(a_{Lx})(a_{Ly})\right]}{\left[1+\frac{2\sigma_e \tau f P_L}{h\upsilon_L w_{Lx} w_{Ly}}(a_{Lx})(a_{Ly})\right]} dxdydz = (L+T)$$

2.50

It is now possible to solve this equation numerically to give the input/output characteristics of the laser as a function of the signal and pump powers $P_L$ and $P_p$.

At threshold the output laser power is zero, i.e. $P_L$=0. Substitution of $P_L$=0 into 2.50 results in an expression for the threshold pump power, $P_{th}$ :

$$P_{th,guide} = \frac{\pi h \upsilon_p}{4\sigma_e \tau f(1-e^{-\alpha_p l})}\left[\left(w_{px}^{\,2} + w_{Lx}^{\,2}\right)^{1/2}\left(\overline{w_{py}}^{\,2} + \overline{w_{Ly}}^{\,2}\right)^{1/2}\right] \times \left[L_{guide} + T + 2N_1^{\,0}\sigma_e l\right] \qquad 2.51$$

where the use of average spot sizes in the non-guided direction is indicated as $\overline{w_y}^{\,2}$ [10] where

$$\overline{w_y}^{\,2} = \frac{1}{l}\int_0^l w(z)^2\, dz \qquad 2.52$$

$L_{guide}$ in equation 2.51 represents the round trip propagation loss exponent, $e^{-L} = \exp(-2\alpha_g l)$, where $\alpha_g$ is the guide propagation loss coefficient at the laser wavelength.

The slope efficiency of a laser, $s\varepsilon$, is the gradient of a plot of output laser power versus input pump power. It is a useful characteristic of the laser and describes how efficiently input pump power is converted into output power. $s\varepsilon$ can be evaluated numerically by finding the required $P_p$ for a range of values of $P_L$ substituted into equation 2.50. Slope efficiency is also discussed in section 2.3.5.

### 2.3.4 Four-level laser systems

To use the laser modelling described in sections 2.3.2 and 2.3.3 to describe a pure four-level waveguide laser the population density of the lower level, and thus the reabsorption loss term must be set to zero. This leads to the following expression:

$$P_{th,guide} = \frac{\pi h \upsilon_p}{4\sigma\tau f(1-e^{-\alpha_p l})}\left[\left(w_{px}^{\,2} + w_{Lx}^{\,2}\right)^{1/2}\left(\overline{w_{py}}^{\,2} + \overline{w_{Ly}}^{\,2}\right)^{1/2}\right] \times \left[L_{guide} + T\right] \qquad 2.53$$

Equation 2.53 agrees with the results from the modelling of four-level lasers found in the literature, [11].

The numerical evaluation of equation 2.50 with $N_1^0$ set to 0 can give the required $P_p$ for a range of values of $P_L$. This allows the calculation of the slope efficiency of four-level laser systems

### 2.3.5 Comparison of bulk and waveguide lasers

To demonstrate some of the advantages of a waveguide laser over a comparable bulk system, the theoretical laser threshold and slope efficiency for each system will now be compared.

Rearranging equation 2.51 to allow for the non-guided circularly symmetric geometry of a longitudinally-pumped bulk laser gives:

$$P_{th,bulk} = \frac{\pi h \upsilon_p}{4\sigma_e f \tau (1 - e^{-\alpha_p l})} \left[ \overline{w^2}_{pbulk} + \overline{w^2}_{Lbulk} \right] \times \left[ L_{bulk} + T + 2N_1^0 \sigma_e l \right] \qquad 2.54$$

If the condition that $w_L \approx w_p$ is set, in order to obtain a good slope efficiency, the pump power threshold is proportional to $\overline{w_p^2}$, the pump spot size radius averaged over the gain medium. Therefore the lowest threshold is obtained using a focusing scheme that minimises $\overline{w_p^2}$. This is achieved by focusing to a beam waist size of:

$$w_{p(L)} = \sqrt{\frac{\lambda_{p(L)} l}{2\sqrt{3}\pi n}} \qquad 2.55$$

where $\lambda_{p(L)}$ is the pump (or laser) wavelength. This is somewhat tighter than confocal focusing. The optimum average spot size is then given by:

$$\overline{w^2_p} = \frac{\lambda_p l}{\sqrt{3}\pi n} \qquad 2.56$$

The threshold obtainable in a bulk laser with these optimum spot sizes is found by substituting 2.56 into 2.54.

$$P_{th,bulk} = \frac{h\upsilon_p l}{4\sqrt{3}\sigma f \pi n(1-e^{-\alpha_p l})}\left(\lambda_p + \lambda_L\right) \times \left(L_{bulk} + T + 2N_1^0 \sigma l\right) \qquad 2.57$$

The ratio of waveguide to bulk laser threshold in the same material is found by division of 2.51 by 2.57:

$$\frac{P_{th,guide}}{P_{th,bulk}} = \frac{\frac{\pi h\upsilon_p}{4\sigma\tau f\left(1-e^{-\alpha_p l}\right)}\left[\left(w_{px}^2 + w_{Lx}^2\right)^{1/2}\left(\overline{w_{py}}^2 + \overline{w_{Ly}}^2\right)^{1/2}\right]\left[L_{guide} + T + 2N_1^0\sigma_e l\right]}{\frac{h\upsilon_p l}{4\sqrt{3}\sigma\tau f n\left(1-e^{-\alpha_p l}\right)}\left(\lambda_p + \lambda_L\right)\left[L_{bulk} + T + 2N_1^0\sigma_e l\right]} \qquad 2.58$$

If the output coupler transmission is set to be equal to twice the round trip cavity loss exponent, L, to ensure a good output efficiency in both cases, then,

$$\frac{P_{th,guide}}{P_{th,bulk}} = \left(w_{px}^2 + w_{Lx}^2\right)^{1/2}\left[\frac{\sqrt{3}\pi n}{l(\lambda_p + \lambda_L)}\right]^{1/2}\left[\frac{3\alpha_g + N_1^0\sigma_e}{3\alpha_b + N_1^0\sigma_e}\right] \qquad 2.59$$

Where $\alpha_g$ and $\alpha_b$ are, respectively, the guide and bulk propagation loss coefficients at the laser wavelength. Using equation 2.59, figures 2.6 and 2.7 illustrate situations in which a waveguide geometry will have the greatest advantage over a bulk system. Equation 2.59 shows that this is usually with long lengths of gain material and small guided spot sizes, however the overall increase in loss in a waveguide may offset the advantages over a bulk system. Waveguide fabrication can result in larger propagation losses than in bulk, meaning $L_{guide} > L_{bulk}$. Therefore every effort must be made to keep waveguide losses to a minimum, preferably below 1dB/cm. A simple calculation (ignoring upconversion, saturation and other effects) of the gain available from a

diode-bar pumped Nd:YAG waveguide with typical spot sizes of 2μm X 1mm and 10W of absorbed pump power leads to 226dB. Experimentally diode-pumped gains of 52dB per Watt of absorbed pump power were obtained in a 5mm length of a 3.8μm thick Nd:YAG waveguide [12]. These values show that at least for Nd:YAG, the gain available from a short length of waveguide sample is so high that propagation losses of ~1dB/cm will not stop laser action, however the loss will affect the performance and efficiency of the device, as shown on the following graphs. Figures 2.6 and 2.7 show curves plotted with different reabsorption loss values ($N_1^0\sigma_e$), corresponding to various laser transitions investigated in this thesis.

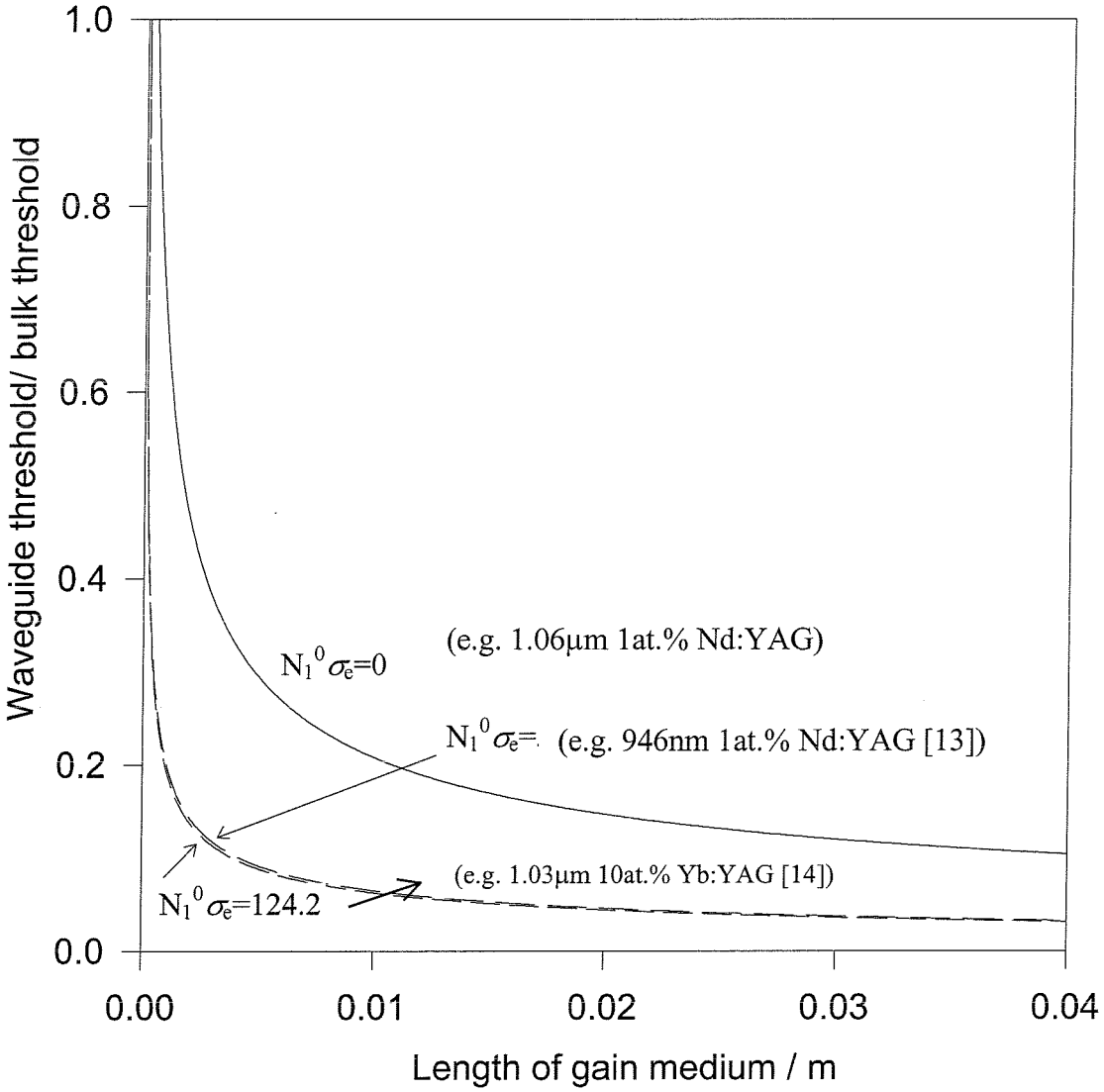


*Figure 2.6* Graph showing the advantage of waveguide geometry over bulk with longer lengths of gain medium

The bulk loss is assumed to be 0.03dB/cm [15], the waveguide loss used is typical for an LPE waveguide, 0.1dB/cm [16], and n=1.82 (for YAG) at 633nm [17]. The guided direction pump and laser spot sizes are set to 2μm and the pump wavelength is 808nm. Figure 2.6 shows that the waveguide geometry has the greatest advantage over bulk for long lengths of gain material.

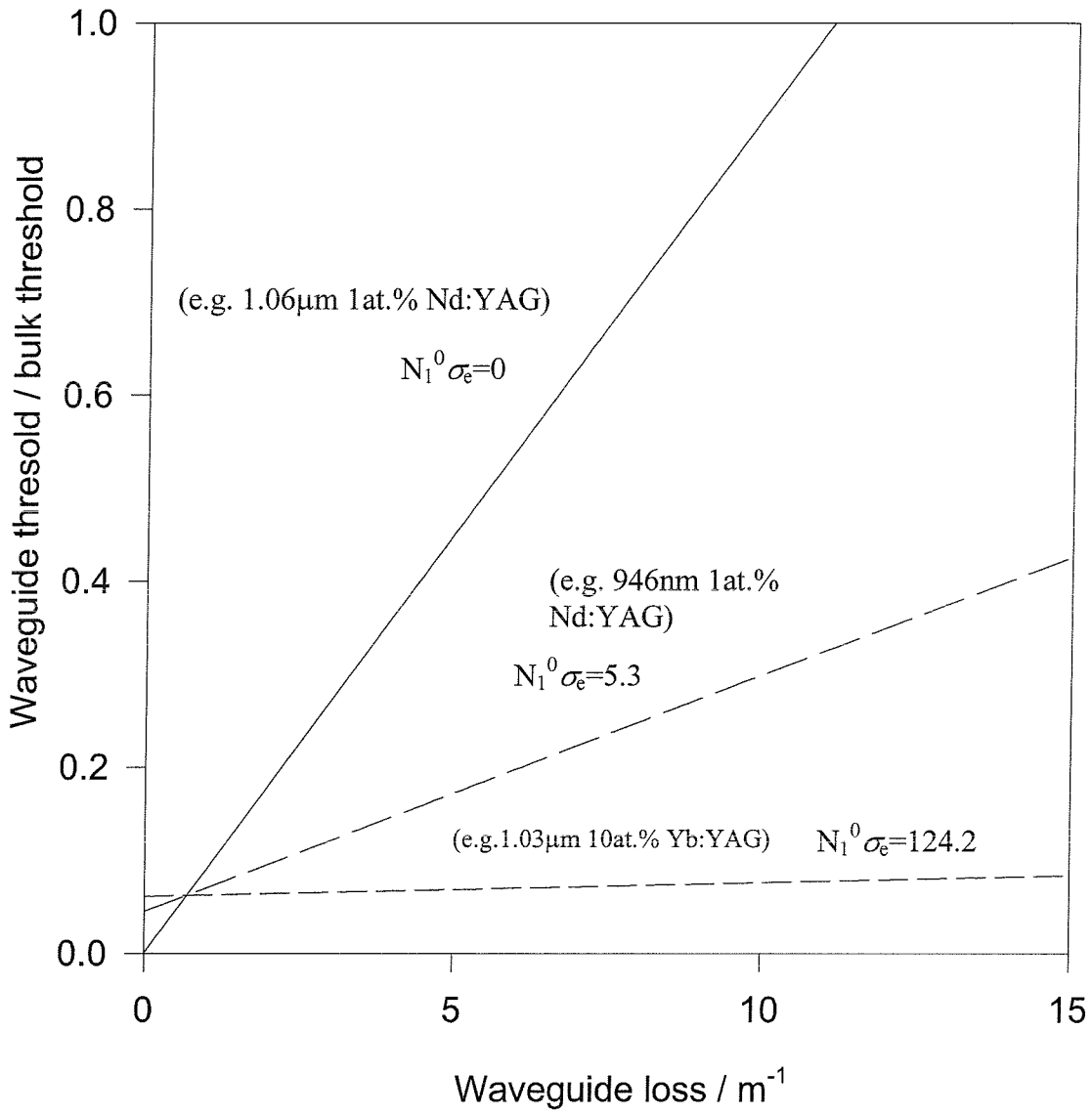


*Figure 2.7* Plots showing advantage of a low loss waveguide laser over a bulk laser

Figure 2.7 illustrates that the benefit of a waveguide geometry is most apparent when using low loss waveguides, the graph is produced for a fixed, 1cm, length of gain medium. One area where propagation losses are less important is in a quasi-three-level laser where the reabsorption losses dominate. The losses in the waveguide are

then comparable to those in the bulk, giving the waveguide a significant advantage. Both figures 2.6 and 2.7 show that a waveguide laser performs comparatively better than a bulk laser for laser systems with higher $N_1^0\sigma_e$ values.

The slope efficiency, $s\varepsilon$, is given by [7]:

$$\frac{dP_L}{dP_p} = s\varepsilon = \left(\frac{T}{T+L}\right)\frac{\upsilon_L}{\upsilon_p}(1-e^{-\alpha_p l})\frac{dS}{dF} \qquad 2.60$$

This ratio depends on: $(1-\exp(-\alpha_p l))$, the absorption efficiency of the incident pump photons, the efficiency of conversion of absorbed pump photons into laser photons (dS/dF), the associated quantum defect, $(\upsilon_L/\upsilon_p)$ and T/(L+T), the fraction of laser photons lost from the cavity through the output coupler compared to the total loss. dS/dF is a quantity that contains the overlap and geometrical factors associated with the conversion of pump photons into laser emission.

The difference in the slope efficiency between a waveguide and a bulk laser is mainly due to the extra propagation loss in the waveguide reducing the laser efficiency. In order to obtain the same slope efficiency from both types of laser system a higher transmission output coupler is required in the waveguide case, but this in turn increases the overall loss in the cavity resulting in a higher laser threshold. However, small spot sizes, a well confined mode and low propagation losses can still combine to result in a waveguide laser with a lower threshold, and the same slope efficiency as a comparable bulk laser.

### 2.3.6 Waveguide laser with uniform population inversion

Modifications are made to the threshold expression given in equation 2.51 for side-pumping, due to the different pump and signal spatial distributions. A side-pumped waveguide laser is shown in figure 2.8, with the doped layer defined by the limits $-d<x<d$, $-l/2<y<l/2$, and $0<z<W$.

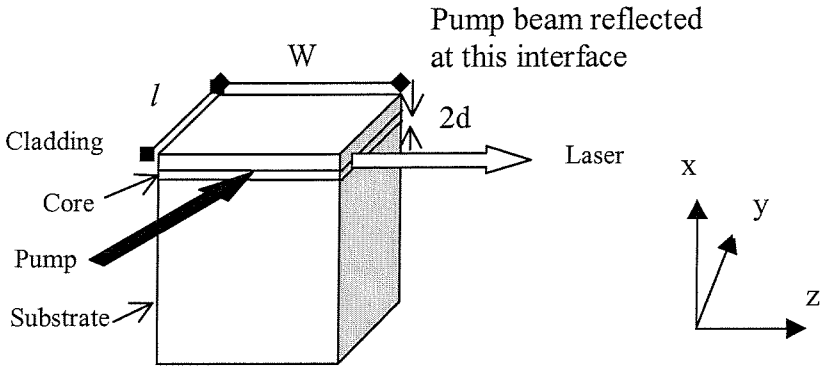


*Figure 2.8* Layout of a side-pumped waveguide laser

The analysis is based on the same principle described earlier in section 2.3.2, however the normalised expressions for the pump distribution, r, and signal distribution, $\phi$, are changed to account for the new pumping geometry. A uniform inversion is assumed, both along the waveguide pumping length, $l$ and the waveguide width, W. This situation approximates the case of a side-pumped waveguide where the pump beam makes a double pass through the gain material, as used later with proximity coupling. Details of this pumping scheme will be given in later chapters. The laser photon distribution is assumed to be invariant along z, but to have fundamental Gaussian modes in the x and y directions. The normalised expressions for $r_0$ and $s_0$ are given in equations 2.61 and 2.62. This analysis assumes that the pump and signal are both well contained within the waveguide core, and so is applicable to the case of a high numerical aperture waveguide.

$$\text{For} \begin{cases} -\infty < x < \infty \\ -l/2 < y < l/2 \\ 0 < z < W \end{cases} \qquad r = \sqrt{\frac{2}{\pi}} \frac{\exp\left(-\frac{2x^2}{w_{px}^2}\right)}{W l w_{px}}$$

elsewhere $r = 0$ 2.61

$$\text{For}\begin{cases} -\infty < x < \infty \\ -\infty < y < \infty \\ 0 < z < W \end{cases} \qquad \phi = \frac{2}{\pi} \frac{\exp - \left( \frac{2x^2}{w_{Lx}^2} + \frac{2y^2}{w_{Ly}^2} \right)}{W w_{Lx} w_{Ly}}$$

elsewhere $s_0 = 0$ 2.62

The threshold of such a three-level laser is obtained by substituting r and $\phi$ into 2.45 and solving for $P_L$=0 as previously. This gives:

$$P_{th} = \frac{\sqrt{\pi} h \upsilon_p l \left[ L_{guide} + T + 2N_1^0 \sigma_e W \right]}{2\sqrt{2} f \sigma_e \tau \left[ 1 - \exp^{-\alpha_p W} \right]} \left( w_{Lx}^2 + w_{px}^2 \right)^{1/2} \qquad 2.63$$

Once again the slope efficiency can be found from numerically solving 2.45 to give the input/output characteristic of the laser

## 2.5 Beam Quality – the $M^2$ measurement

In recent years the topic of laser beam quality has seen much debate within the laser community. A measurement of 'beam quality' is clearly required to fully quantify a laser beam, however it is not yet a solidly defined technical term and its measurement can be carried out in a number of ways. Standards [18] are being developed and tested which will hopefully lead to a uniform, less ambiguous approach to describing a laser beam in the future. A theoretical discussion of $M^2$ beam quality will be given here, as the second moment based $M^2$ values have been used to describe beam quality in the majority of this thesis. The experimental technique used for these measurements can be found in the next chapter (section 3.10).

It is important to know how a beam will behave as it propagates through the elements in a laser cavity. In particular how the beam focuses after a lens is crucial to laser design. A fundamental Gaussian mode will focus to the minimum possible waist diameter and diverge least on passing through a lens. It has diffraction-limited

performance. A measurement of $M^2$ beam quality can be made by analysing how an arbitrary beam diverges and focuses compared to this diffraction-limited behaviour.

### 2.5.1 Measuring beam width

In order to compare the divergence of an arbitrary beam to that of a diffraction limited beam, and thus find an $M^2$ value, a method of defining and measuring the beam width must be found.

A popular technique measures the radius, r, at which the intensity falls to $1/e^2$ of some peak intensity, however this is only valid for Gaussian beams with $M^2=1$ and not for beams containing higher order modes [19].

A more mathematically rigorous definition uses the second moment of the beam intensity distribution I(r).

This is defined as [19]:

$$\overline{r^2} = \frac{\int_{-\infty}^{\infty} (r - r_0)^2 I(r) dA}{\int_{-\infty}^{\infty} I(r) dA} \qquad 2.64$$

where A is the area over which the integration is performed, and $r_0$ is the centre of gravity of the beam.

For a beam with circular symmetry equation 2.64 becomes [19]:

$$\overline{r^2} = \frac{2\pi \int_{-\infty}^{\infty} r^3 I(r) dr}{\int_{-\infty}^{\infty} I(r) dA} \qquad 2.65$$

and the spot size radius, $W_r$, (defined as the $1/e^2$ radius of a Gaussian profile) is related to the second moment as in equation 2.66:

$$W_r = \sqrt{2\overline{r^2}} \qquad 2.66$$

However if a beam, for example a diode-bar, is non-circularly symmetric it is useful to express equation 2.64 in rectangular co-ordinates. The second moment of the beam intensity distribution I(x,y) across the co-ordinate x (or y) is:

$$\overline{r_x^2} = \frac{\int_{-\infty}^{\infty}\int_{-\infty}^{\infty}(x - x_0)^2 I(x,y)dxdy}{\int_{-\infty}^{\infty}\int_{-\infty}^{\infty} I(x,y)dxdy} \qquad 2.67$$

where $x_0$ is the centre of gravity of the beam.

This second moment obeys a rigorous, universal free-space propagation rule [19, 20]:

$$\overline{r_x^2(z)} = \overline{r_{0x}^2} + \overline{r_\theta^2} \times (z - z_0)^2 \qquad 2.68$$

where $r_{0x}$ is the variance at the beam waist, $r_\theta$ is the variance of the angular spread of the beam from the waist and $z_0$ is the position of the beam waist along the z axis. This quadratic propagation dependence has been found to be true for all types of laser beams; Gaussian or non-Gaussian, single or multi-transverse mode. However equation 2.68 is only rigorously true when beam widths are defined by the second moment of intensity method. Any attempt to universally define or measure beam quality must therefore use second moments beam widths.

Substituting a Gaussian beam profile, described by, $I(x)=\exp[-2x^2/w_x^2]$, into equation 2.67 gives $w_x = 2\sqrt{r_x^2}$. This is detailed in equations 2.69-2.71.

$$\overline{r_x^2} = \frac{\int_{-\infty}^{\infty} x^2 e^{-2x^2/w_x^2} dx}{\int_{-\infty}^{\infty} e^{-2x^2/w_x^2} dx} \qquad 2.69$$

using the standard integrals

$$\int_{-\infty}^{\infty} e^{-ax^2} dx = \sqrt{\frac{\pi}{a}} \qquad \int_{-\infty}^{\infty} x^2 e^{-ax^2} dx = -\frac{d}{da}\sqrt{\frac{\pi}{a}}$$

and setting $\frac{2}{w_x^2} = a$

$$\text{gives } \overline{r_x^2} = \frac{-\frac{d}{da}\sqrt{\frac{\pi}{a}}}{\sqrt{\frac{\pi}{a}}} = \frac{1}{2a} \qquad 2.70$$

$$\text{thus } w_x = \sqrt{4\overline{r_x^2}} \qquad 2.71$$

For a beam that is separable in the x and y directions:

$$< \overline{r^2} >=< \overline{r_x^2} > + < \overline{r_y^2} > \qquad 2.72$$

$$\text{which gives: } < \overline{r^2} >= \frac{w_r^2}{4} + \frac{w_r^2}{4} \qquad \text{and thus} \qquad w_r = \sqrt{2\overline{r^2}}$$

in agreement with the circularly symmetric beam width given in equation 2.66.

It is then logical to define the spot size or beam width, W, of an arbitrary beam as:

$$W_x \equiv \sqrt{4\overline{r_x^2}} \qquad W_y \equiv \sqrt{4\overline{r_y^2}} \qquad 2.73$$

The beam widths, $W_x$ and $W_y$, based on second moments will propagate in free space as a Gaussian spot (of size w(z)) would do, except the far-field spreading of the beam would be multiplied by a factor $M^2$. The beam width of any arbitrary beam defined in this way can then be written [20]:

$$W_x^2(z) = W_{0x}^2 + M_x^4 \times \left(\frac{\lambda}{\pi W_{0x}}\right)^2 (z - z_{0x})^2 \qquad 2.74$$

and

$$W_y^2(z) = W_{0y}^2 + M_y^4 \times \left(\frac{\lambda}{\pi W_{0y}}\right)^2 (z - z_{0y})^2 \qquad 2.75$$

where $M_x$ and $M_y$ are characteristic parameters of the particular beam. The near-field far-field product can be written using $M_x$ and $M_y$ as in equations 2.76.

$$W_{0x} \times W_x(z) \approx M_x^2 \times \frac{z\lambda}{\pi} \qquad W_{0y} \times W_y(z) \approx M_y^2 \times \frac{z\lambda}{\pi} \qquad 2.76$$

Thus the $M^2$ value gives a measure of the 'quality' of an arbitrary beam and poor quality, less ideal beam profiles will have larger near-field far-field products, i.e. $M^2>1$. Using this convention an arbitrary laser beam can be fully characterised in both directions with the six parameters; $W_{0x}$, $W_{0y}$, $z_{0x}$, $z_{0y}$, $M_x^2$, $M_y^2$.

The overall beam quality of a laser depends on the laser design itself, for instance the shape of the cavity, the emitting area and thermal effects in the gain medium. For example diode lasers have a highly astigmatic emitting region. The output from this region is non-diffraction limited in the non-guided direction, leading to a large difference in $M^2$ values in the x and y directions. $M^2$ is also affected by aberrations introduced by optics used to focus and direct the output beam. Methods of spatial mode control for improving the output laser beam quality of a waveguide laser will be discussed in chapter 7.

## 2.6 References

[1] A.Yariv, *'Quantum Electronics'*, Chap.13, Wiley (1989)

[2] D.H.Lee, *'Electromagnetic Principles of Integrated Optics'*, Chap.4, Wiley (1986)

[3] A.W.Snyder. J.D.Love, *'Optical Waveguide Theory'*, Chaps.1-5, Chapman and Hall (1983)

[4] D.H.Lee, *'Electromagnetic Principles of Integrated Optics'*, Chap.5, Wiley (1986)

[5] H.J.W.M.Hoekstra, G.J.M.Krijen, P.V.Lambeck, Opt. Comm., **94**, pp.506-508 (1992)

[6] C.L.Bonner, T.Bhutta, D.P.Shepherd, A.C.Tropper, IEEE J. Quantum Electron., **36**, pp.236-242 (2000)

[7] W.P.Risk, J. Opt. Soc. Am. B, **5**, pp.1412-1423 (1988)

[8] K.Kubodera, K.Otsuka, J. Appl. Phys., **50**, pp.653-659 (1979)

[9] T.Y.Fan, R.L.Byer, IEEE J. Quantum Electron., **23**, pp.605 612 (1987)

[10] M.F.J.Digonnet, C.J.Gaeta, Appl. Opt., **24**, pp.333-342 (1985)

[11] W.A.Clarkson, D.C.Hanna, J. Modern Optics, **36**, pp.483-498 (1989)

[12] D.P.Shepherd, C.T.A.Brown, T.J.Warburton, D.C.Hanna, A.C.Tropper, B.Ferrand, Appl. Phys. Lett., **71**, pp.876-878 (1997)

[13] D.C.Hanna, A.C.Large, D.P.Shepherd, A.C.Tropper, I.Chartier, B.Ferrand, D.Pelenc, Appl. Phys. Lett., **63**, pp.7-9 (1993)

[14] P.Lacovara, H.K.Choi, C.A.Wang, R.L.Aggarwal, T.Y.Fan, Opt. Lett., **16**, pp.1089-1091 (1991)

[15] T.Nishimura, T.Omi, Jpn. Appl. Phys., **14**, pp.1011 (1975)

[16] I.Chartier, B.Ferrand, D.Pelenc, S.J.Field, D.C.Hanna, A.C.Large, D.P.Shepherd, A.C.Tropper, Opt. Lett., **17**, pp.810-812 (1992)

[17] D.Pelenc, *'Guide d'onde laser en Nd:YAG et Yb:YAG per E.P.L.'*, PhD Dissertation, Département Optronique du LETI, C.E.N.G. 85X 38041, France (1992)

[18] ISO/DIS standard 11 146, *'Optics and Optical Instruments, Lasers and Laser related equipment, Test methods for laser beam parameters'*, International Organisation for Standardisation, P.O. Box 65, CG1211, Geneve, Switzerland (1997)

[19] M.W.Sasnett Chap. 9. pp.132-142, *'The Physics and Technology of Laser Resonators'* D.R.Hall, P.E.Jackson, eds., IOP Publishing, (1989)

[20] A.Seigman, *'How to (maybe) measure laser beam quality'*, TUL1, Tutorial at OSA Annual meeting, Long Beach, California, USA, 12-17 October (1997)